Microwave Loss in the High-Performance Dielectric $Ba(Zn_{1/3}Ta_{2/3})O_3$ at 4.2 K

Lingtao Liu,[1] Marco Flores,[2] and Nathan Newman[1,*]

[1]*Materials Program, SEMTE, Arizona State University, Tempe, Arizona 85287, USA*

[2]*Department of Chemistry and Biochemistry, Arizona State University, Tempe, Arizona 85287-1604, USA*

(Received 3 August 2012; published 18 December 2012)

Temperature- and magnetic-field-dependent measurements of the loss tangent in $Ba(Zn_{1/3}Ta_{2/3})O_3$ doped with transition metals (Mn, Ni) are compared to those from samples doped with other impurities (Cd, Ga, Mg, and Zr). These results, combined with pulsed electron paramagnetic resonance measurements, show conclusively that microwave loss in transition-metal-doped $Ba(Zn_{1/3}Ta_{2/3})O_3$ at cryogenic temperatures is attributable to resonant spin excitations of unpaired transition-metal d electrons in isolated atoms (light doping) or exchange coupled clusters (moderate to high doping), a mechanism that differs from the usual suspects.

DOI: 10.1103/PhysRevLett.109.257601 PACS numbers: 77.22.Gm, 61.72.J−, 76.30.−v, 77.84.−s

Condensed matter theoreticians have developed tools that can accurately predict intrinsic and extrinsic physical properties of solid-state materials [1]. This demonstrates that there is a strong understanding of the underlying mechanisms responsible for their electronic, optical, magnetic, chemical, thermal, and structural characteristics. However, a fundamental understanding of what determines one of the most important parameters, the loss tangent, has still not been established, especially in practical high performance dielectrics.

Researchers to date have identified several processes that can cause microwave loss, including absorption by free carriers [2,3], electron paramagnetic resonance [4], anharmonic phonons [5–9], two-level systems with precession of electric dipoles in polar molecules [10,11], and nonresonant spin excitations in exchange coupled transition-metal defect complexes [12,13]. The important question is which of these, if any, is responsible for microwave loss in practical microwave dielectrics.

This work investigates $Ba(Zn_{1/3}Ta_{2/3})O_3$ (BZT), a low loss tangent ($< 2 \times 10^{-5}$ scaled to 2 GHz) and high dielectric constant (~ 30) material that can be tuned with $\sim$12% Ni doping on the Zn site to achieve a microwave device zero temperature coefficient of resonant frequency [14]. A small fraction of $BaZrO_3$ is often alloyed with this compound since it improves the manufacturability of the material by allowing shorter annealing times to achieve low loss [14]. Interest in high dielectric-constant low loss dielectrics is of great technological importance. Losses in dielectric resonators and filters limit the performance of most microwave communication and radar systems. One strategy to reduce loss is to operate these dielectrics at reduced temperatures. If optimized for cryogenic temperatures, the use of these materials could potentially also positively impact quantum computing, photonic detector, amplifier, and mixer circuitry, as the performance of these advanced electronics is often limited by ac losses and the associated noise [15,16].

Recent reports of the loss tangent of practical microwave materials have found a variety of behavior ranging from a strong increase to a significant drop in the loss tangent at low temperatures [17–21]. An understanding of the dominant loss mechanism under these conditions is lacking and is the focus of this study. Our approach is to quantitatively measure the temperature- and magnetic-field-dependent loss tangent of undoped and doped BZT using microwave resonators whose quality factors (Q's) are limited by dielectric loss. These results, combined with pulsed electron paramagnetic resonance (EPR) measurements, have allowed us to identify the dominant mechanism of microwave loss in transition-metal-doped BZT at low temperatures.

Undoped and Cd-, Ga-, Mg-, Mn-, Ni-, and Zr-doped BZT ceramic samples were synthesized using conventional solid-state powder processing techniques [22] in our lab. $Ba[(Zn_{1-x}Ni_x)_{1/3}Ta_{2/3}]O_3$ ceramic samples were synthesized over a range of compositions with x ranging from 0 to 0.6. X-ray diffraction measurements confirmed that $Ba(Zn_{1/3}Ta_{2/3})O_3$ and $Ba(Ni_{1/3}Ta_{2/3})O_3$ form a miscible solid solution without phase separation. In this alloy system, Zn and Ni share the common B' site in the $A(B'_{1/3}, B''_{2/3})O_3$ complex perovskite structure. For brevity, we denote the composition of the alloy by the fraction of Ni on the B' site (i.e., 0–60% in this study) henceforth.

Microwave measurements to infer the dielectric loss tangent are performed in transmission using parallel plate resonator (PPR) [23] and dielectric resonator (DR) techniques. An HP8510C microwave network analyzer is used to source an electromagnetic wave and then measure S21 vector values. These values are fit to a circle in the Smith chart to infer the quality factor Q. The distance between coupling loops and sample is adjusted to be weakly coupled to infer the unloaded Q within a few percent. For each measurement, a PPR or DR is then loaded into a 2.03 cm $\times$ 0.61 cm $\times$ 1.52 cm gold-plated copper cavity, which is affixed to the end of a cryogenic dipping probe. This probe is inserted either into a helium dewar for 4 K measurements

without a field or in a cryostat (PPMS, Model 6000, Quantum Design, San Diego, CA) for temperatures as low as 2 K and magnetic fields as high as 9 T.

The PPR technique uses two superconducting $YBa_2Cu_3O_{7-\delta}$ films on 10 mm × 10 mm buffered sapphire substrates to form the parallel plates with a BZT-based sample as the interlayer dielectric. For our measurements, the interlayer dielectric is made sufficiently thick (i.e., 0.5 mm) so that the dielectric losses dominate [24].

DR measurements are made using 8.5 mm × 6.5 mm × 2 mm rectangular resonators, and also gave high Q values indicating that radiation and near field losses for this configuration also do not significantly affect the measurement result. Continuous wave (cw) EPR spectra were recorded at liquid helium temperatures using a Bruker ELEXSYS E580 continuous wave X-band spectrometer (Bruker, Silberstreifen, Germany) equipped with an Oxford Model 900 EPL liquid helium cryostat (Oxford Instruments, Oxfordshire, UK). The magnetic field modulation frequency was 100 kHz, the amplitude was 1 mT, the microwave power was 1 mW, the microwave frequency was 9.42 GHz, and the sweep time was 168 s. Pulsed X-band (9.7 GHz) EPR measurements were performed at 4 K using a Bruker ELEXSYS E580 FT−EPR X-band spectrometer equipped with an Oxford flow-cryostat CF 935 and a dielectric ring resonator (ER 4118X-MD5). Field-swept electron-spin-echo detected EPR spectra were recorded using the two-pulse echo sequence ($\pi/2$-τ-π-τ-echo). Microwave pulses of 8 ns ($\pi/2$) and 16 ns (π) and $\tau = 140$ ns were used. The spin-lattice relaxation time (T_1) was obtained from inversion recovery experiments. The phase-memory time (T_2^*) was measured by the Hahn echo decay method.

cw EPR spectra were simulated using EasySpin (v 4.0.0) [25]. The spectra of lightly to moderately doped samples were modeled considering two different single Ni^{2+} ion ($S = 1$) species, whereas those of heavily doped samples were modeled considering only a spin system with $S = 2$. Fitting was performed with the three g values, g_x, g_y, and g_z, the linewidth, ΔB, the zero-field splitting parameters, D and E, and the fitting procedures of Flores and co-workers [26]

The quality factor Q and the corresponding loss tangent of samples measured at 4 K are found to strongly depend on the concentration of Mn and Ni dopants, i.e., transition-metal impurities, as shown in Fig. 1. Note that BZT with dopants such as Cd, Ga, Mg, and Zr without unpaired d electrons do not exhibit the same degradation in the Q when compared with the other samples. These data clearly show that the presence of "magnetic" dopants, such as Ni and Mn, play a dominant role in the microwave loss mechanism in these transition-metal containing materials at 4.2 K.

Fitting the low-field magnetic susceptibility data to the Curie-Weiss law indicates that all of the Ni-doped samples exhibit antiferromagnetic ordering at different temperatures. Table I summarizes the inferred Weiss temperature. The

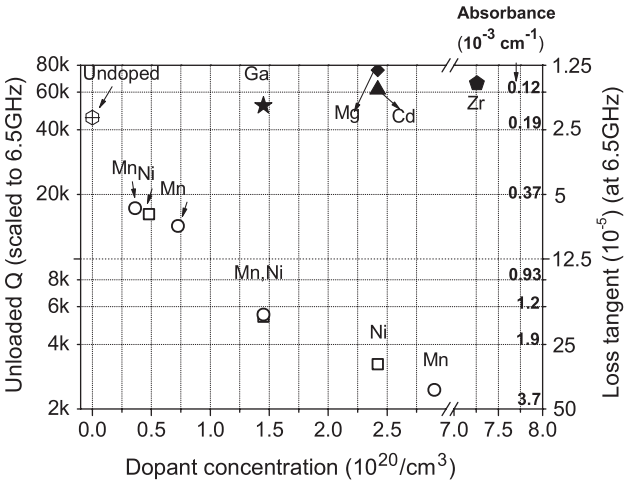

FIG. 1. Unloaded Q factor and loss tangent of BZT doped with various impurities measured with the parallel plate resonator configuration at 4.2 K and no applied magnetic field.

Weiss temperature is expected to be a close estimate of the Neel temperature in this work, as the large separation between Ni atoms in this work indicates that the spin interactions between atoms more distant than the nearest neighbors will be inconsequentially small. A decreasing trend in the effective moment, $\mu_{\text{eff}}[= g_j\sqrt{J(J+1)}]$, in terms of the number of Bohr magnetrons (μ_B) per Ni atom is found for the larger Ni contents, as shown in Table I. This is additional evidence of magnetic interactions between Ni at higher impurity concentrations.

Figure 2 presents the quality factor of the resonators and the inferred loss tangent and absorbance for the materials at 4.2 K. As can readily be observed, the loss tangent of the Ni-doped samples depends strongly on a magnetic field for samples with 8% and greater Ni content. This indicates that loss is related to the spin degree of freedom in these samples. Phonons do not have a net charge or contain a magnetic moment and would thus not be expected to exhibit significant magnetic field dependence [2].

The high Q's obtained enhance our ability to measure the loss tangent accurately and thus detect trace levels of absorption, including that from EPR [27,28]. EPR signals were detected at several magnetic fields; these can readily be observed as wide dips (peaks) in the Q (loss tangent). For instance, peaks at 1350, 1650, 3350, and 8000 G were observed for the 1 and 8% samples in Figs. 2(a) and 2(b). This is substantiated by cw EPR measurements (first derivative) with smaller steps in the magnetic field taken with a conventional EPR spectrometer (see below); see Fig. 2(c). Integration of the EPR derivative spectra produces results that are in agreement with the DR loss tangent measurements. The signals present in the EPR spectra were modeled using spectral simulations [29]. Two main Ni^{2+} (d^8, $S = 1$) species were identified in the 1 and 8% samples (see Supplemental Material, Fig. S1 [30]). One species, characterized by a broad signal centered at ~8000 G, was

TABLE I. Magnetic properties of BZT doped with different Ni concentrations.

Ni concentration (cm^{-3})	Fraction of Ni on Zn site	Average Ni separation (Å)	From temperature-dependent low-field magnetic susceptibility measurements (characteristic of all unpaired electrons) $\mu_{\text{eff}} = g_j\sqrt{J(J+1)}$ per Ni atom (μ_B)	Weiss temperature (K)	From fitting Brillouin function to magnetic-field-dependent susceptibility measurements (characteristic of clusters) J (measurement temperature in K)	M_s (emu/cm^3) $\{g_jJ\}$
5.2×10^{19}	1%	27	3.11	0.5	0.65 (4.2)	0.9, {1.9}
4.1×10^{20}	8%	13	2.97	1.4	1.5 (4.2)	7.7 {2.1}
1.0×10^{21}	20%	9.9	3.03	1.8	2 (10)	20 {2.2}
2.1×10^{21}	40%	7.9	2.96	3.3	3 (15)	40 {2.2}
3.1×10^{21}	60%	6.9	2.97	4.6	4 (20)	64 {2.4}
4.1×10^{21}	80%	6.2	2.94	6.4	10 (20)	87 {2.4}

fit with an isotropic g value of 2.20 and zero field splitting parameters, D and E, of 64.9 and 0 GHz, respectively. The broadening of this signal is because of dipolar spin-spin interactions. The second species presents signals at low-magnetic field ($\sim$ 1000 G) that were fit using 1.95, 2.39, 2.16, 12.5, and 4.16 GHz for g_x, g_y, g_z, D, and E, respectively. Both species correspond to a substitutional Ni^{2+} in an octahedral crystal ligand field, with no rhombic distortion ($E/D = 0$) for the first one and maximum rhombic distortion ($E/D = 1/3$) for the second one [31]. The EPR spectra of the 1 and 8% samples also show signals centered at 3370 G ($g = 2.00$). The large intensity sharp feature was simulated using a $S = 1/2$ species with $g = 2.00$ and was tentatively attributed to free carriers presumably in local isolated regions (since the samples do not exhibit a measurable dc conductivity). The nearby features with smaller intensity were simulated considering a $S = 1$ species with isotropic $g = 2.00$, $D = 1.3$ GHz, and $E = 0$ GHz. They were not assigned to Ni^{2+} since the value of g does not match that of Ni^{2+} (typically $\sim$2.20).

Some aspects of the Ni^{2+} EPR signals change markedly as the doping concentration increases, while others do not. The spectral features from the low-magnetic-field species are not significantly altered, except for the amplitude, with the increase in Ni concentration. Such behavior shows that this species corresponds to isolated Ni^{2+} ions, which are not present in samples with 40% Ni and higher doping. In our lightly doped samples, the low-field EPR peak from isolated Ni species with the maximum rhombic distortion ($E/D = 1/3$) extends down to the zero applied field and dominates the loss there. Resonant loss from paramagnetic centers has been proposed to play a significant and often dominant role at reduced temperatures in ultralow-loss crystalline materials, including sapphire [4].

In contrast, the features of the broad signal species change with doping concentration. Its resonance field position decreases, and its linewidth increases with increasing Ni concentration (see Supplemental Material, Table S1 [30]). The broad signal completely dominates the EPR spectra of samples with Ni concentration above 20%. Its spectra can be simulated with an $S = 2$ spin system and an enhanced value of D. Although exchange interactions were not used in the simulations because of the large broadening; they can also be involved in the spectral changes. Thus, the spectral changes induced by the increase in Ni concentration are associated with the formation of "clusters," in which the exchange interactions between Ni^{2+} ions that are situated in the regular atomic lattice are orders of magnitude larger than dipolar interactions. Therefore, in our heavily doped samples, the dominant species are clusters of Ni^{2+} ions.

We now focus on the properties of the resonant spin process in which the $3d$ electron spins of Ni and Mn clusters are coupled through an exchange interaction to produce a "super spin." Then we show that the magnetic field dependence of our data is consistent with this mechanism.

Gesmundo and Rossi [32] have shown that transition-metal clusters act as a single spin when the exchange energy $Js_1 \cdot s_2$ is greater than the Zeeman interaction $g\beta H$. The total spin quantum number is a sum of the spins, $S = s_1 + s_2 + s_3 + \cdots + s_n$ and can take on integral values from 0 to S [32] with corresponding energies of $S(S+1)J$ [i.e., 0, $2J$, $6J$, $12J$, $20J$, $30J$, $42J$, ...]. The dipole-dipole interaction between the spins of these clusters results in the broadening of the level as a result of the number of neighbors statistically increase as the square of the distance and the interaction decreases as the inverse cube [13].

Gesmundo and Rossi showed that in $Ni_xMg_{1-x}O$ alloys, the super spin clusters were coupled for Ni atoms at distances of $\sim$8 Å and less (i.e., Ni-doping levels of $2 \times 10^{21}/cm^3$). It is interesting that the average Ni separation in our 40% Ni sample is on the order of 8 Å and the 4.2 K loss drops most sharply at large magnetic fields for this and higher Ni concentration samples, presumably from decoupling when the Zeeman energy dominates over the exchange energy. The Q's in moderate to high transition-metal-doped BZT exposed to large fields that are as high and even higher

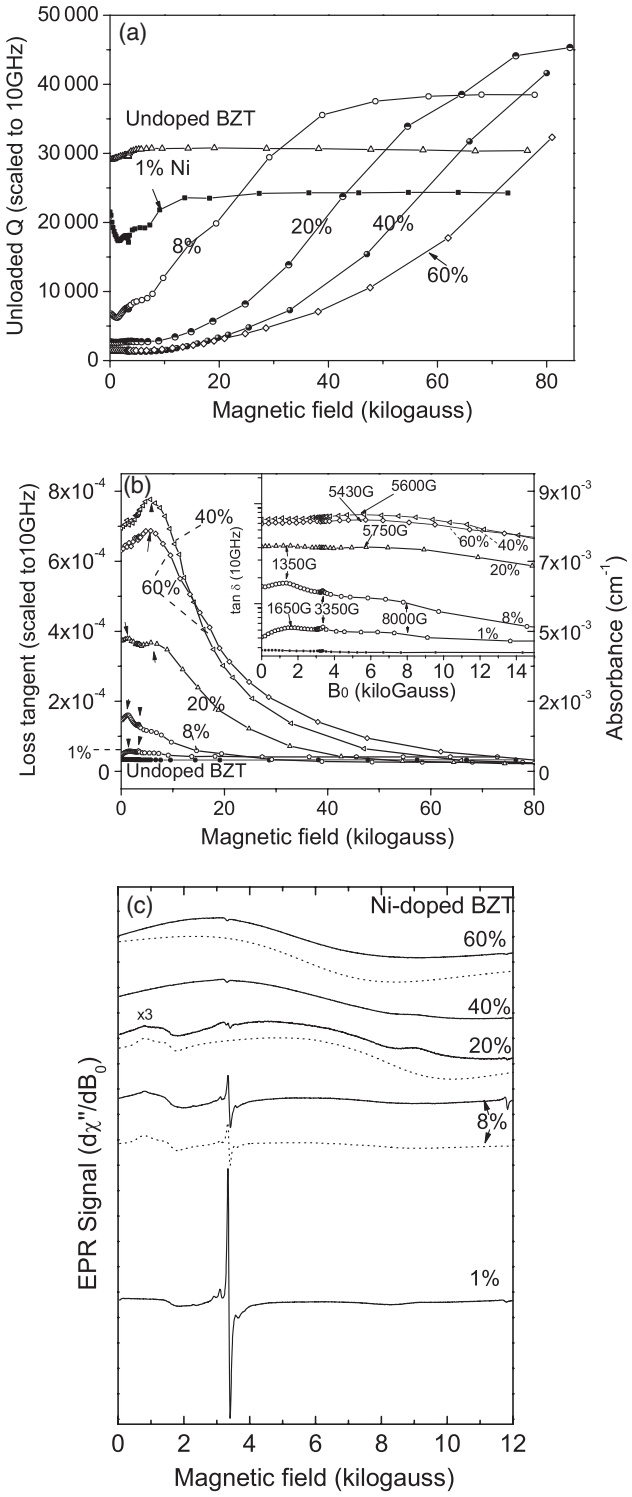

FIG. 2. (a) Measured Q and (b) inferred loss tangent and absorbance of Ni-doped ceramic BZT at 4.2 K measured using the dielectric resonator configuration. The inset is an expanded view at low fields. Arrows point at EPR resonant absorption peak maxima. For comparison, (c) illustrates conventional CW EPR spectra (derivative of absorbance) of the ceramic (polycrystalline) samples measured using a Bruker EPR spectrometer. Solid lines denote experimental data and dotted lines denote spectra simulations.

than obtained otherwise suggests that these materials could potentially be optimized to realize improved performance under these conditions.

Note that the undoped and 1%-doped Ni samples do not show a strong magnetic field dependence. For samples with Ni concentrations below $5 \times 10^{19}/\mathrm{cm}^3$, with average separations of 27 Å, as found in our 1 and 8% samples, Gesmundo and Rossi's work suggests that the Ni present should act as isolated ions. This hypothesis has been confirmed in our EPR experiments (see above). Now, we can attribute the loss in samples with higher concentrations to be dominated by increasing broadened lines resulting from peaks associated with the super spin clusters.

To give a more direct estimate of the average number of transition-metal impurities involved in the clusters for each Ni-doped sample, field-dependent magnetic susceptibility data were fit to the J of the Brillouin function. Although we do not understand why the 1% Ni sample has such a small value (as isolated d^8 Ni^{2+} atoms typically have a J of $\sim$1.4), the trend in the fitted J does show that the "average" cluster size increases from a little less than 1 for the 1% Ni-doped sample, 1.5 for 8%, 2 for 20%, 3 for 40%, 4 for 60%, and 10 for 80%. These data suggest that exchange coupling of $3d$ electrons into higher spin clusters occurs in samples doped with 8% and larger Ni content—the exact same samples that show the marked increase in Q and the corresponding drop in the loss tangent at high-magnetic fields.

Furthermore, the field-swept electron-spin-echo detected EPR spectra also showed a peak in absorption at low-magnetic fields, down to near zero applied magnetic field, for the 1, 8, and 20% Ni-doped samples at 4 K (see Supplemental Material, Fig. S2 [30]). Determinations of the spin-lattice relaxation time (T_1) and the phase-memory time (T_2^*) in this broad low-field peak for the respective samples indicated that the peak belongs to a fast-relaxing species and suggests that the pulsed spectra are all inhomogeneously broadened. The times measured at the lowest observed field (20–50 G) range from 1 to 5 μs for T_1 and 90 to 650 ns for T_2^*. The observation of an electron spin Hahn echo within the low-field peak, which extends from hundreds of gauss down to zero field unquestionably demonstrates that the absorption process involves localized electron spin flips (i.e., EPR transitions) and rules out the possibility of absorption by spin-polarized transport over an intermediate barrier, by tunneling (as suggested by Ref. [2]), or by the nonresonant spin excitation process that results in a low-magnetic field absorption peak over an energy width of $J/\hbar$, as described by Bleaney and Ingram [12,13]. Spin-polarized transport, free carriers, and electric dipole precessions would also not be expected to exhibit the magnetic field dependence on loss tangent observed in our study.

Our more recent measurements [33] for a wider range of ceramics (including commercial transition-metal-doped

$Ba(Zn_{1/3}Ta_{2/3})O_3$, $Ba(Zn_{1/3}Nb_{2/3})O_3$, and $BaTi_4O_9$-$BaZn_2Ti_4O_{11}$) also exhibit a marked increase in the low temperature loss tangent attributable to the same mechanism. The results also demonstrate that this mechanism significantly contributes to room temperature loss, but does not dominate.

In conclusion, we have shown that microwave loss in transition-metal-doped BZT at low temperature is attributable to resonant spin excitations of unpaired d electrons within isolated impurity atoms for small dopant concentrations and within exchange coupled clusters for higher concentrations.

We would like to thank David Cronin, Michael Thorp, and Ralph Chamberlin for insightful discussions and the Army Research Office for support of this work under Contract No. W911NF-11-1-0508. The use of facilities in the LeRoy Eyring Center for Solid State Science (LE-CSSS) at Arizona State University is also acknowledged.

*Corresponding author.
nate.newman@asu.edu

[1] The reader is referred to the past few decades of the modern solid-state literature including Physical Review B, Condensed Matter Physics, Advances in Physics, Journal of Physics: Condensed Matter, Physical Review Letters, and Physics Today.
[2] N. W. Ashcroft and N. D. Mermin, *Solid State Physics* (Holt, Rinehart, and Winston, Philadelphia, PA, 1976), pp. 2–27, 416–450, 626, and references therein.
[3] R. R. Rakhimov, E. M. Jackson, D. E. Jones, and G. B. Loutts, J. Appl. Phys. **95**, 5653 (2004).
[4] V. B. Braginsky, V. P. Mitrofanov, and V. I. Panov, *Systems with Small Dissipation* (University of Chicago, Chicago, 1985).
[5] H. Tamura, D. A. Sagala, and K. Wakino, Jpn. J. Appl. Phys. **25**, 787 (1986).
[6] H. Tamura, Am. Ceram. Soc. Bull. **73**, 92 (1994).
[7] K. Wakino, M. Murata, and H. Tamura, J. Am. Ceram. Soc. **69**, 34 (1986).
[8] V. L. Gurevich and A. K. Tagantsev, Adv. Phys. **40**, 719 (1991).
[9] K. R. Subbaswamy and D. L. Mills, Phys. Rev. B **33**, 4213 (1986).
[10] M. von Schickfus and S. Hunklinger, J. Phys. C **9**, L439 (1976).
[11] D. P. Pappas, M. R. Vissers, D. S. Wisbey, J. S. Kline, and J. Gao, IEEE Trans. Appl. Supercond. **21**, 871 (2011).
[12] B. Bleaney and J. E. Ingram, Proc. R. Soc. A **208**, 143 (1951).
[13] A. Abragam and B. Bleaney, *Electron Paramagnetic Resonance of Transition Ions* (Oxford University, New York, 1970), pp. 514–518.
[14] P. K. Davies, J. Tong, and T. Negas, J. Am. Ceram. Soc. **80**, 1727 (1997).
[15] J. M. Martinis, K. B. Cooper, R. McDermott, M. Steffen, M. Ansmann, K. D. Osborn, K. Cicak, S. Oh, D. P. Pappas, R. W. Simmonds, and C. C. Yu, Phys. Rev. Lett. **95**, 210503 (2005).
[16] M. P. Weides, J. S. Kline, M. R. Vissers, M. O. Sandberg, and D. S. Wisbey, Appl. Phys. Lett. **99**, 262 502 (2011).
[17] J. Konopka, I. Wolff, and S. J. Lewandowksi, J. Appl. Phys. **72**, 218 (1992).
[18] M. R. Varma and N. D. Kataria, J. Mater. Sci. **18**, 441 (2007).
[19] H. Tamaura, H. Matsumoto, and K. Wakino, Jpn. J. Appl. Phys. **28**, 21 (1989).
[20] J. Kanopka and I. Wolff, IEEE Trans. Microwave Theory Tech. **40**, 2418 (1992).
[21] J. Krupka, R. G. Geyer, M. Kuhn, and J. H. Hinken, IEEE Trans. Microwave Theory Tech. **42**, 1886 (1994).
[22] S. Liu, R. Taylor, N. S. Petrovic, L. Budd, M. Van Schilfgaarde, and N. Newman, J. Appl. Phys. **97**, 014105 (2005).
[23] R. C. Taber, Rev. Sci. Instrum. **61**, 2200 (1990).
[24] L. Liu, Arizona State University, Ph.D. dissertation, 2012.
[25] S. Stoll and A. Schweiger, J. Magn. Reson. **178**, 42 (2006).
[26] M. Flores, R. Isaacson, E. Abresch, R. Calvo, W. Lubitz, and G. Feher, Biophys. J. **92**, 671 (2007).
[27] F. J. Rosenbaum, Rev. Sci. Instrum. **35**, 1550 (1964).
[28] W. M. Walsh and L. R. Rupp, Rev. Sci. Instrum. **57**, 2278 (1986).
[29] B. Kirste, in *Handbook of Electron Spin Resonance. Data Sources, Computer Technology, Relaxation, and ENDOR*, edited by C. P. Poole and H. A. Farach (American Institute of Physics Press, New York, 1994), Chap. 2, p. 33.
[30] See Supplemental Material at http://link.aps.org/supplemental/10.1103/PhysRevLett.109.257601 for theoretical fits of the EPR features in the experimental data.
[31] J. Krzystek, A. Ozarowski, and J. Telser, Coord. Chem. Rev. **250**, 2308 (2006).
[32] F. Gesmundo and P. F. Rossi, J. Solid State Chem. **8**, 287 (1973).
[33] L. Liu, A. Matusevich, C. Garg, and N. Newman, Appl. Phys. Lett. (to be published).